ARTICLES

Differential Cross Section for Rotationally Inelastic Scattering of Vibrationally Excited NO(v=5) from Ar

Amitavikram A. Dixit, Patrick J. Pisano, and Paul L. Houston*

Department of Chemistry and Chemical Biology, Cornell University, Ithaca, New York 14853

Received: June 19, 2001; In Final Form: August 29, 2001

Rotationally inelastic scattering of vibrationally excited NO(v=5) from Ar was studied with a crossed molecular beam ion-imaging apparatus. Vibrationally excited NO was generated at the exit of a pulsed nozzle by the photoinitiated reaction between O(^{1}D) and N_2O. The results for rotational excitation in vibrationally excited NO were compared to those in the vibrational ground state at a collision energy of 1460 cm^{-1}. The final rotational state of NO, populated by scattering from Ar, was detected by 1 + 1 REMPI via the A($^2\Sigma^+$) ← X($^2\Pi_{1/2}$) electronic transition. The R_{21} transition was used to probe the final scattered state in both cases. The rotational rainbow maxima are observed at slightly smaller angles in the scattering of vibrationally excited NO from Ar compared to the scattering of NO in the vibrational ground state from Ar. A hard-ellipse potential model was used to investigate the effect of initial vibrational excitation on the rotational energy-transfer process. The small shifts observed in the rainbow maxima are evidence for a slight enhancement in angular anisotropy in the intermolecular potential for NO(v=5)/Ar compared to that for NO(v=0)/Ar.

Introduction

The scattering of NO from rare gases has served as a model system for understanding the energy-transfer mechanism in a molecule with a Π electronic ground state. The extensive experimental study of inelastic scattering of NO from rare gases is complemented by a general theoretical framework for inelastic collisions of molecules in the Π electronic ground state.[1−4] Inelastic collisions have been studied with an increasing degree of detail in an effort to understand the mechanism of energy transfer.

In one of the earliest studies, Thuis et al. determined the total scattering cross section for state-selected NO.[5] A hexapole was used to select NO molecules in the $j = \Omega = m_j = {}^3/_2$ state. A pair of magnet coils defined the direction of the quantization axis in the measurements as either parallel or perpendicular to the direction of the relative velocity vector. The anisotropy was defined in terms of the cross sections measured for the two orientations of the quantization axis. A single potential surface of the form $V_0(R) + V_2(R)\, P_2(\cos\theta)$ was used to describe the angular dependence of the intermolecular potential and to model the experimentally observed anisotropy. Subdo and Loy measured state-to-state integral rate constants using an IR−UV double-resonance (IRUVDR) technique in a gas-cell experiment.[6,7] They measured the rate constants, at room temperature, for rotational energy transfer in NO induced by collisions with Ar, N_2, CO and SF_6. Andresen and co-workers measured state-to-state integral cross sections for collisions of NO with Ar in a crossed molecular beam apparatus.[8,9] The final scattered products were detected by laser-induced fluorescence (LIF). More recently, rate constant measurements for collisional relaxation in NO have been extended to lower temperatures.[10−14] In these studies, rotational energy transfer in NO with moderate vibrational excitation was studied. For example, rotational energy transfer in NO(v=3) was studied by James et al.,[13] who used a specially designed Laval nozzle to produce a flow of gas that was uniform in temperature, density, and velocity. This innovation made it feasible to measure rate constants at temperatures down to 7 K. The accompanying theoretical calculations agreed to within experimental error for the NO/Ar system.

Each rotational level in the NO molecule has a fine structure of two nearly degenerate energy levels that are referred to as the Λ doublet components. Alexander predicted a propensity for collisions to populate the Π(A′) Λ doublet state provided that the final state of the scattered product NO has some Hund's case b character.[15] Experimental measurements of the integral cross section with Λ doublet parity selection, either for the initially prepared state prior to scattering[16] or for the final state populated by scattering,[17] confirm this propensity. Recently, the role of the orientation of NO in collisions with Ar has been examined.[18,19] The NO molecule was not only prepared in a particular Λ doublet state but also oriented by an electric field relative to the incident Ar beam. This enabled the authors to examine collisions occurring predominantly from the N end or the O end of the molecule.

Recently, Wodtke et al. measured the integral cross sections for rotational energy transfer in collisions of vibrationally excited NO (v = 20) with He.[20] The parity-selected initial state was prepared by stimulated emission pumping (SEP), and the final state was detected by laser-induced fluorescence. NO was assumed to be a rigid rotor with a bond length set equal to the average bond length for the v = 20 level in the theoretical treatment. Close-coupled quantum scattering calculations for this system matched reasonably well with the experimental observations.

10.1021/jp012318z CCC: $20.00
Published on Web 11/22/2001

Another observable that characterizes the scattering process is the differential cross section, which provides a sensitive probe of short-range anisotropy in the intermolecular potential. Keil et al. were the first to measure the differential cross section for a NO/rare gas system in a crossed molecular beam study.[21] A quadrupole mass spectrometer was used to detect the scattered He at different angles. Since then, different laser-based detection schemes have been used to measure the differential cross section. Imaging techniques in conjunction with state-selective ionization have been used to measure the differential cross section.[22−25] The imaging technique offers the advantage of providing the complete angular distribution of scattered products for selected final rotational levels. Jons and co-workers used laser-induced fluorescence to determine the differential cross section in the scattering of NO from Ar in a crossed molecular beam apparatus.[26,27] Quantum scattering calculations performed for the different NO/rare gas systems are generally in good agreement with the experiments.[15,28,29] A recent experimental and theoretical investigation[30] of the bound states of the Ar−NO complex found good agreement between the experimental peaks and the positions predicted by a CCSD(T) potential.[29] Likewise, the steric effect in Ar/NO collisions has been investigated experimentally and compared successfully to theory.[31]

For the NO/rare gas system, no measurement of the differential cross section for rotational energy transfer in vibrationally excited NO has been reported. However, the effect of vibrational excitation on the rotational energy-transfer process has been studied in rare gas/alkali dimer systems. For example, the differential cross section for the $Na_2(v=31)$/Ne system was measured by Ziegler et al.[32] The experiment was carried out in a crossed molecular beam apparatus, and the scattered products were detected by LIF at different laboratory angles using a rotatable detector. For a given rotational transition, the rotational rainbow for the $Na_2(v=31)$/Ne system was found to peak at a smaller angle compared to that for the $Na_2(v=0)$/Ne system. The anisotropy in the interaction potential determines the angle of the observed rainbow. Thus, an increased anisotropy was calculated for the $Na_2(v=31)$/Ne system compared to the $Na_2(v=0)$/Ne system.

The aim of the current study was to examine the influence of vibrational excitation on the rotational-energy-transfer process in the NO/Ar collisional system. The velocity-mapped ion-imaging technique[33] was used in a crossed molecular beam apparatus. The scattered NO was state-selectively detected by a 1 + 1 REMPI scheme. The differential cross section for the NO($v=5$)/Ar system was then compared to that for the NO($v=0$)/Ar system at the same collision energy.

Experimental Section

A crossed molecular beam ion-imaging apparatus previously described[34] was used for the scattering experiment. The design of the apparatus enables generation of radicals at the exit of a pulsed piezoelectric nozzle. Vibrationally excited NO was generated from the reaction between $O(^1D)$ and N_2O. A study of this reaction has been reported earlier.[35] Helium flowed over a silica-gel trap held at a dry ice/2-propanol bath temperature and charged with O_3 and N_2O. The precursor mixture of O_3/N_2O/He was then expanded through a pulsed piezoelectric nozzle at a backing pressure of 1 psig. The O_3 was photolyzed at 266 nm at the exit of the nozzle to generate $O(^1D)$. Typically, the energy of the photolysis laser was 30 mJ, and the photolysis laser beam was focused at the exit of the nozzle with a lens of approximately 65 cm focal length. The beam of NO thus generated intersected a beam of Ar at 90° at the center of the scattering chamber. The Ar beam was expanded at a backing pressure of 1 psig. Rotationally inelastic scattering of NO($v=5$) from Ar was compared to that of NO($v=0$) from Ar at the same collision energy.

NO scattered into different final rotational states was state-selectively ionized by a 1 + 1 REMPI scheme via the $A(^2\Sigma^+) \leftarrow X(^2\Pi_{1/2})$ electronic transition. Only spin multiplet-conserving collisions were studied. The wavelength range used to probe rotational excitation in NO($v=5$) was between 264.5 and 267 nm, whereas that for NO($v=0$) was between 224.7 and 226.2 nm. The R_{21} transition was used in both cases to probe the final rotational state. The frequency-doubled output of a XeCl excimer (LPX 210i, Lambda Physik) pumped dye laser (FL2002, Lambda Physik) produced approximately 1 mJ/pulse in the two wavelength regions. The relative delay time between the photolysis laser and the probe laser was set to maximize the signal of NO($v=5$) that was probed at the center of the chamber. The velocity of the radical beam was then calculated on the basis of this time of flight and the distance between the photolysis point and the center of the chamber. This velocity, along with that calculated for the argon beam, allowed the collision energy for the NO($v=5$)/Ar system to be calculated. To obtain the same collision energy for the NO($v=0$) experiments, a 0.1% NO/He/Ar gas mixture was employed.

The NO product ions were extracted by a set of ion optics perpendicular to the plane of the two molecular beams and were velocity mapped onto a Galileo MCP/phosphor detector.[33] The output from the detector was recorded by a CCD camera (Xybion CCD-50). The experiment was run at 10 Hz, and the image acquisition was controlled by a program written in Labview (National Instruments).[34] The inelastic scattering signal was obtained by toggling the Ar beam between on and off states after every 20 shots and taking the difference of signals. This procedure corrects for any background population that is present in the radical beam. The image was acquired by scanning the probe-laser wavelength across the rotational peak to correct for the Doppler spread in wavelengths for the scattered NO. At each wavelength in the Doppler-scanned image, 200−300 acquisitions were collected, depending on the signal level. Each acquisition for a given final rotational level then consists of two separate images corresponding to the two toggle states used for the Ar beam, each scanned over the Doppler profile of the rotational level. The net image, which displays the angular distribution for the rotationally inelastic scattering of NO from Ar, is the difference of these two separate images.

Results

Rotationally inelastic scattering was studied at a collision energy of 1460 cm^{-1} for the NO($v=5$)/Ar system. The study was carried out at the same collision energy for the NO($v=0$)/Ar system to determine whether differences arise in the angular distributions as a result of the differing vibrational excitation of the diatomic. The reaction between $O(^1D)$ and N_2O results in a distribution of vibrationally excited NO that peaks in intensity close to $v = 5$.[35] The relative population of NO in $v = 5$ is approximately 15%. The final rotational state populated by scattering was probed by 1 + 1 REMPI via the $A(^2\Sigma^+) \leftarrow X(^2\Pi_{1/2})$ electronic transition. The spectral peak was chosen such that only one rotational level was probed. The NO spectrum for $A(^2\Sigma^+, v'=1) \leftarrow X(^2\Pi_{1/2}, v''=5)$ was assigned on the basis of LIFBASE program,[36] and line positions were predicted using the molecular constants cited in the work by Zachwieja et al.[37] Angular distributions for rotational excitation to three different final states, $j = 6.5$, 16.5, and 20.5, were obtained for the two systems NO($v=5$)/Ar and NO($v=0$)/Ar.

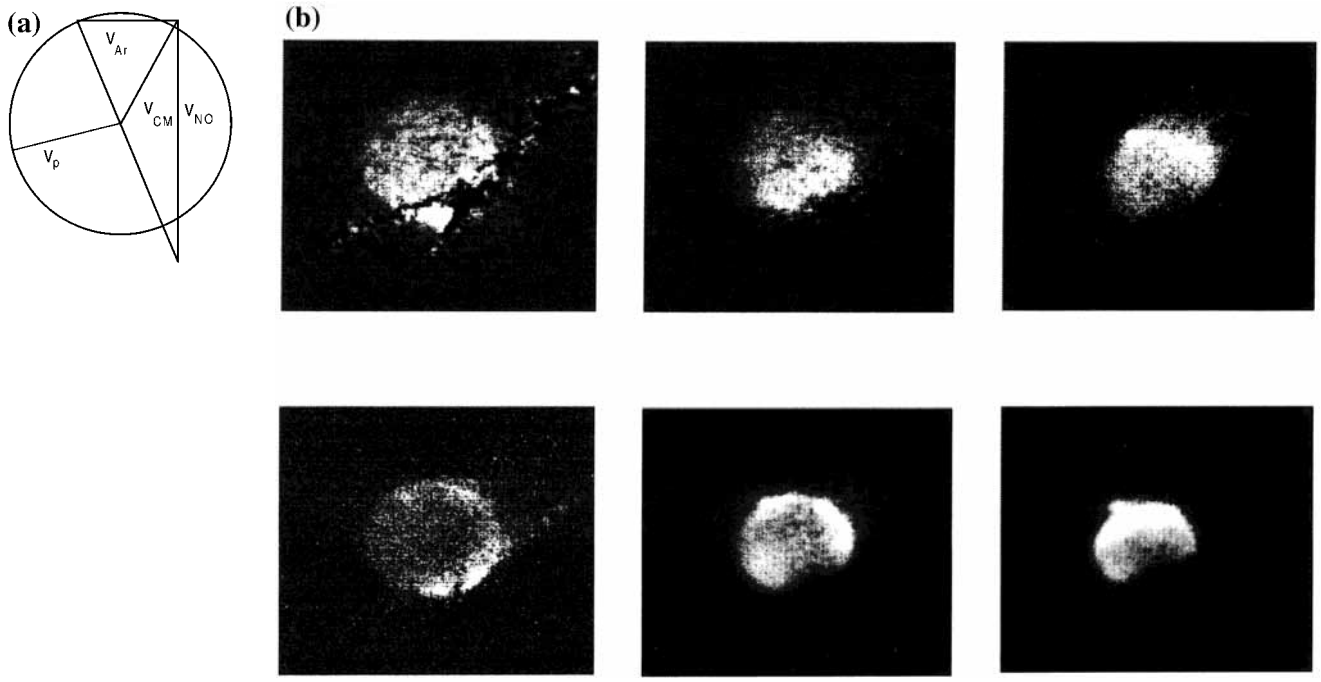

Figure 1. (a) Newton diagram for NO/Ar scattering. (b) Data images for $v = 5$, $j = 6.5$, 16.5, and 20.5 and $v = 0$, $j = 6.5$, 16.5, and 20.5. Upper panel: (left) $v = 5$, $j = 6.5$; (middle) $v = 5$, $j = 16.5$; (right) $v = 5$, $j = 20.5$. Lower panel: (left) $v = 0$, $j = 6.5$; (middle) $v = 0$, $j = 16.5$; (right) $v = 0$, $j = 20.5$.

Figure 1 shows the images for scattering into the three final rotational states for the two cases. The accompanying Newton diagram shows the directions of the NO and Ar beams in the image. As can be seen from the orientation of the Newton diagram, the forward-scattered signal is closer to the lower right-hand corner, whereas the backward-scattered signal is closer to the upper left-hand corner of the image. Because the contribution to the signal due to population in the radical beam prior to collision is subtracted to obtain the net image, there is an absence of intensity in the forward direction that corresponds to the position where the NO beam maps onto the detector. The images qualitatively convey the features of the differential cross section. For both the systems, the intensity in the angular distribution shifts to the backward direction with increasing rotational excitation. Such behavior is indicative of the collisional system probing the repulsive interaction potential.

Discussion

Although the images convey the qualitative form of the differential cross section, the detection setup introduces certain artifacts that convolute with the true angular distribution. First, the image has a low signal-to-noise ratio in the forward direction where the NO beam maps onto the detector. The net signal, derived by subtracting the contribution of background NO signal, is sensitive to the subtraction of two large numbers. Second, a velocity-dependent bias in detection is introduced by the detection scheme. The gas pulses have a wider temporal profile ($\sim$300 μs) than the laser pulse ($\sim$10 ns). Also, the volume traversed by the probe laser is smaller than the volume common to the intersecting beams. Because of these constraints, products from scattering events that occurred as early as a few microseconds before the laser fires can be detected. Scattered products from an event preceding the firing of the laser are more likely to be detected if they have small laboratory velocities than large laboratory velocities. Third, the ion signals arising from scattering at the edges of the effective field are not perfectly velocity-mapped. This problem shows up as a trail of intensity extending out of the Newton sphere. Finally, it should be noted that the image is the two-dimensional projection of the three-dimensional differential cross section.

To correct for these experimental biases to the differential cross section, a forward simulation method, described elsewhere,[25,34] is used to model the apparatus and extract the true angular distribution. The differential cross section (DCS) is varied in successive iterations to generate a simulated image, and iterations are carried out until the simulated image matches the data image. The intensity enclosed in an annulus at the outer edge of the Newton sphere corresponds to the angular distribution skewed by the apparatus function. The annular integration of this intensity for different scattering angles is compared for both the data and the simulated image to determine the quality of fit and convergence of the simulation.

We have investigated the error propagation in our images by changing the number of counts by $\pm\sqrt{N}$, where N is the number of counts in each pixel, and then seeing how the differential cross section varies. In the forward direction, where we need to take the difference between two large numbers to obtain the image, the error in the differential cross section can approach $\pm$10%. In the backward direction, it is less than $\pm$5%. In another check, a hard-ellipse differential cross section (with two rainbow peaks) was used to generate an image, and the differential cross section was then re-extracted. The re-extracted DCS agreed well with the original, showing that the error introduced by the procedure is very small.

Figure 2, which shows the data image and simulated image for $v = 5$, $j = 20.5$, provides an example of the process. The extracted differential cross sections for all final rotational states are plotted in Figures 3 and 4. Oscillations on the scale of 5°, such as in the $j = 20.5$ cross section, are likely to be noise due to a finite binning size, whereas those observed in $j = 6.5$ are likely to be real. The differences between $v = 0$ and $v = 5$ for $j = 16.5$ and for $j = 20.5$ at wide angles are likely to be real, as our analysis indicates that the error in this region is less than 5%. The rotational rainbow peaks are sharper and more forward-

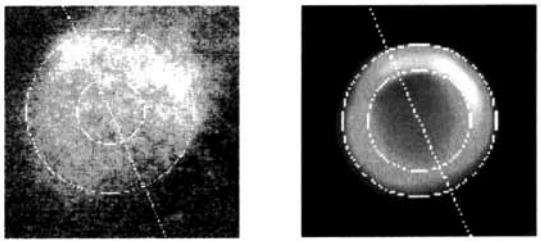

Figure 2. (Left) Data image for $v = 5$, $j = 20.5$. (Right) Simulated image for $v = 5$, $j = 20.5$.

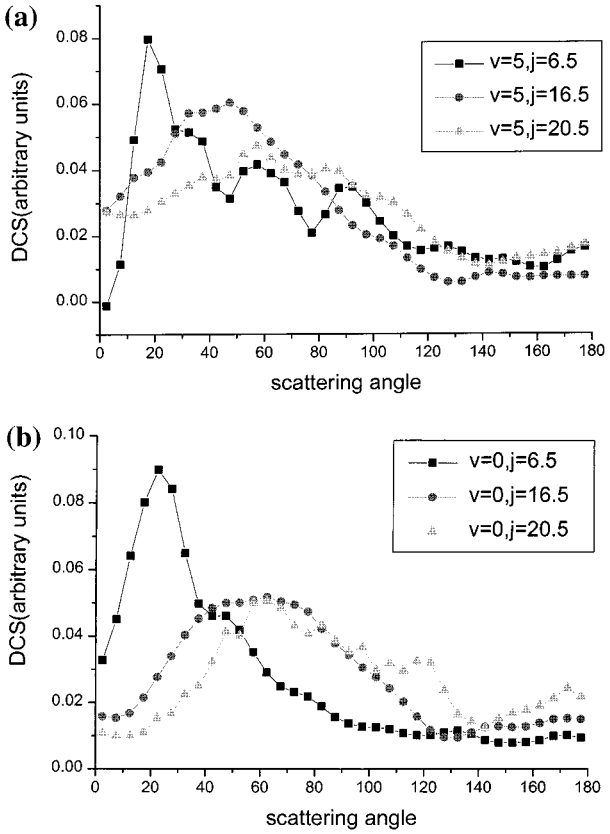

Figure 3. (a) Plot of differential cross section (DCS) for $v = 5$, $j = 6.5$, 16.5, and 20.5. (b) Plot of DCS for $v = 0$, $j = 6.5$, 16.5, and 20.5.

scattered for $j = 6.5$ and then progressively more backward-scattered for $j = 16.5$ and 20.5. In all cases, the $v = 0$ peaks seem to be slightly more backward-scattered than the corresponding $v = 5$ peaks. We believe these features to be consistent and outside our error limits. Surprisingly, the 0° forward scattering for $v = 5$, $j = 6.5$ is actually smaller than the 0° scattering for $j = 16.5$ and 20.5, and this appears to be outside our error limit of 10%. Nonetheless, the overall scattering is still more forward in the case of lower changes in j than higher ones.

For both $v = 0$ and $v = 5$ excitations of NO, the differential cross section exhibits a rotational rainbow peak that shifts to larger scattering angle with increasing rotational excitation. Such behavior can be modeled by scattering from a repulsive interaction potential. The two-dimensional hard-ellipse model provides a classical description of the atom/diatom scattering process and emphasizes the importance of the repulsive interaction potential.[38,39] In this model, the repulsion is modeled by treating the diatom as a hard ellipse. The semimajor and semiminor axes of the ellipse are defined using the potential energy contour for the atom/diatom system at the collision energy under study. The semimajor and semiminor axes of the ellipse equal the positions of the contour along the bond axis

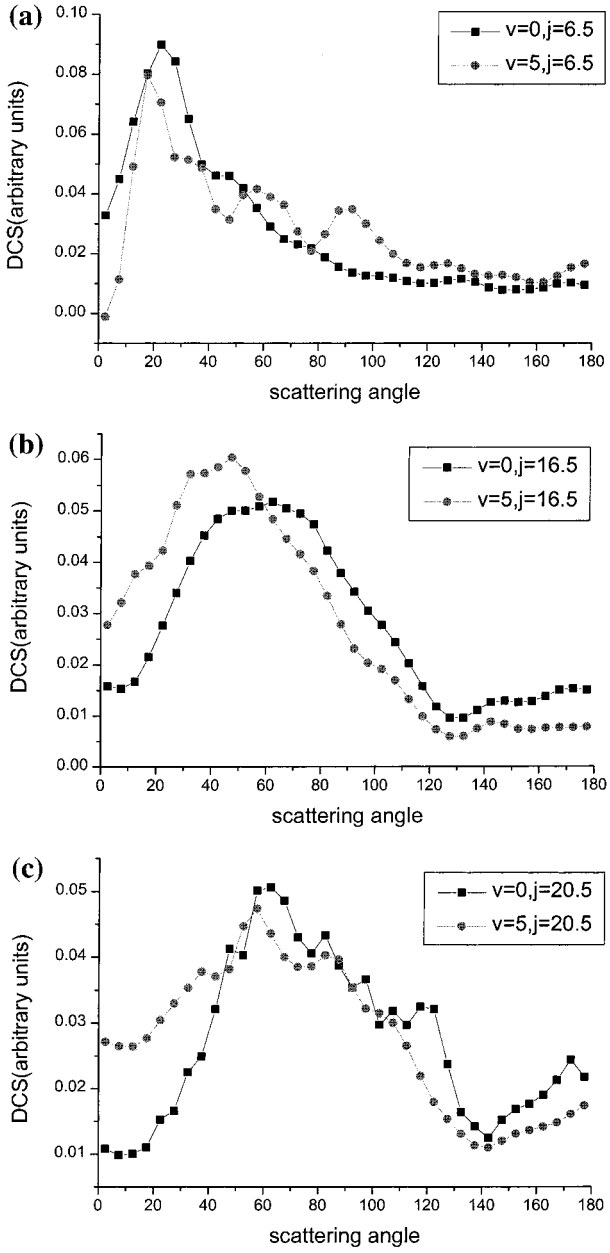

Figure 4. (a) Plot of DCS for $v = 5$, $j = 6.5$ and $v = 0$, $j = 6.5$. (b) Plot of DCS for $v = 5$, $j = 16.5$ and $v = 0$, $j = 16.5$. (c) Plot of DCS for $v = 5$, $j = 20.5$ and $v = 0$, $j = 20.5$.

and perpendicular to the bond axis, respectively. For a homonuclear diatomic with $\epsilon = \mu/I \ll 1$, the rainbow angle θ_R is given by the expression

$$\sin(\theta_R/2) = \Delta j/[2(A - B)] \qquad (1)$$

where $\Delta j = j/p_0$; j is the final angular momentum of the rotor; p_0 is the initial linear momentum; and A and B are the semimajor and semiminor axes of the ellipse, respectively. This simple relation predicts that the rainbow angle bears an inverse relation to the angular anisotropy, $A - B$, in the potential.

The differential cross section for a particular final rotational state in the NO(v=5)/Ar system is compared to that in the NO(v=0)/Ar system in Figure 4. For a fixed final rotational state, the DCS curves are very similar for the two cases, and the rainbow maximum for the NO(v=5)/Ar system is very close to that for the NO(v=0)/Ar system. However, in all cases, the rainbow maximum for the NO(v=5)/Ar system appears to be

shifted slightly toward the forward direction compared to that for the NO(v=0)/Ar system. NO is nearly a homonuclear diatomic, and if real, the small shift in rainbow position toward smaller rainbow angle for the NO(v=5)/Ar system could be qualitatively rationalized on the basis of the increased average bond length for NO(v=5) and the simple relation, eq 1, described earlier. If $A - B$ increases slightly as a result of the increase in the average bond length, one should observe a small shift toward smaller rainbow angle for the NO(v=5)/Ar system. One should view this explanation with caution, however, as eq 1 is strictly valid for $\epsilon = \mu/I \ll 1$, whereas for NO, $\epsilon = 1.724$ Å^{-2}.

A more rigorous approach would involve a quantum scattering calculation using an interaction potential for the NO(v=5)/Ar system. In the study of rotational energy transfer in NO(v=20) scattered from He, Wodtke et al.[20] calculated a potential energy surface for the scattering system by treating the NO molecule as a rigid rotor. The bond length of NO was set equal to the average bond length for the $v = 20$ level. The theoretically predicted integral cross sections matched reasonably well with the experimental data.

Because a similar potential energy surface is not available for the NO(v=5)/Ar system, we used the hard-ellipse model to gain a qualitative understanding of how the scattering should depend on vibrational level. We used the exact equations for a two-dimensional hard-ellipse model to predict the differential cross section for the two systems NO(v=5)/Ar and NO(v=0)/Ar.[38,39] Under the approximation that there is no difference, δ, between the center of symmetry and the center of mass, the results of the calculation are shown in Figure 5. Incorporation of the value of $\delta = 0.1$ Å for NO and convolution with our experimental resolution showed that we should have seen a double rainbow for both $j = 16.5$ and $j = 20.5$, but not for $j = 6.5$. Indeed, a slight shoulder in the NO(v=0)/Ar data for $j = 20.5$ might indicate the residual of a double rainbow, but it appeared that both peaks predicted for $j = 16.5$ fell under the observed broad maximum around 60°. We thus set $\delta = 0$ in the calculation and focused on the differences caused by the change in vibrational level.

Ellipse parameters were estimated for both the NO(v=0)/Ar and NO(v=5)/Ar systems. For the NO(v=0)/Ar system, these parameters were taken from the appropriate potential energy contour on the ab initio potential energy surface.[15] These ellipse parameters were then iteratively varied to find the best fit for the experimentally observed rainbow positions for the three final rotational states. The best fit parameters for the NO(v=0)/Ar system were close to the initial choice and were found to be $A = 3.35$ Å and $B = 2.95$ Å. Using a Morse oscillator potential for NO, the average bond lengths were calculated for the $v = 0$ and $v = 5$ levels and found to be 1.155 and 1.202 Å, respectively. For the NO(v=5)/Ar system, the increase in the average bond length due to the vibrational excitation was added to the previously determined A parameter of the ellipse for the NO(v=0)/Ar system. The B parameter used for the NO(v=5)/Ar system was the same as that for the NO(v=0)/Ar system. The predicted differential cross sections for the two cases are plotted in Figure 5.

The rainbow peaks predicted for the NO(v=5)/Ar system lie at smaller angles than those for the NO(v=0)/Ar system. With increasing rotational excitation, the rainbow peaks for the two cases move further apart. This trend is clearly evident in the experimentally derived differential cross section when comparing $j = 6.5$ to $j = 16.5$ (see Figure 4). It is harder to see this trend when comparing $j = 16.5$ to $j = 20.5$ because the differential cross section becomes broader for the latter final rotational state. If the rising and falling edges of the differential cross section are compared in the $j = 20.5$ case, the trend for increasing separation between the rainbow peaks with increasing rotational excitation seems to prevail. The small shift in the rainbow angles in the NO(v=5)/Ar system toward smaller angles is evidence for a slight enhancement in angular anisotropy in the intermolecular potential arising as a result of moderate vibrational excitation.

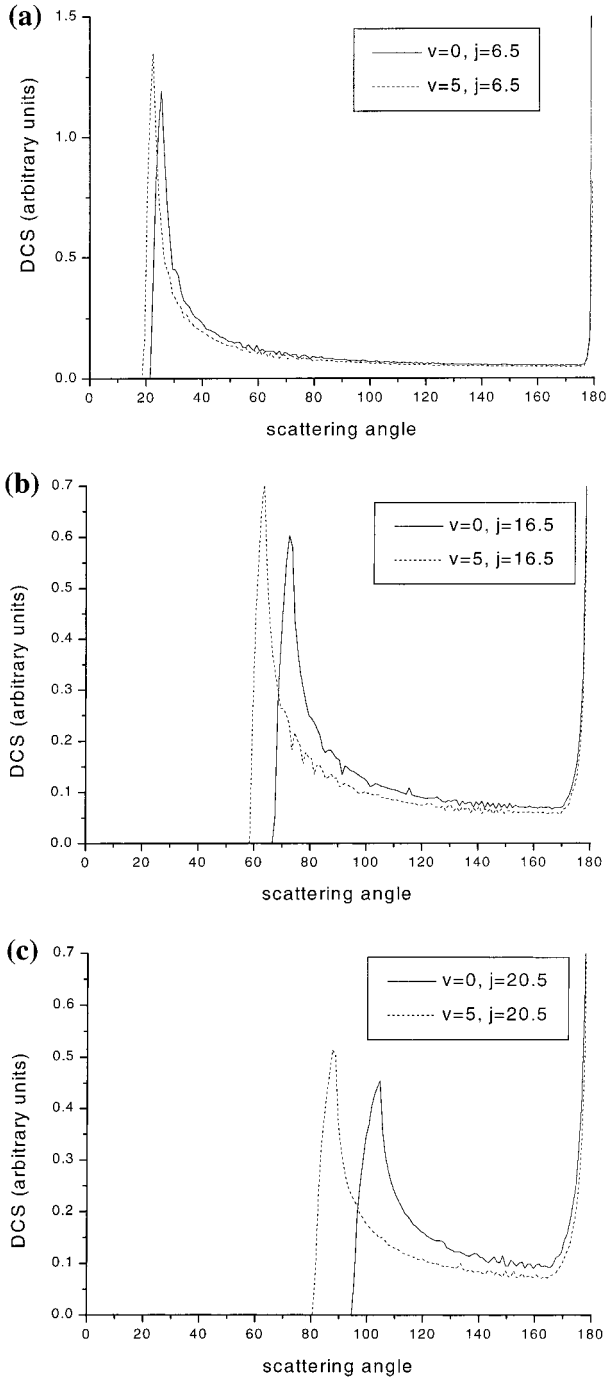

Figure 5. DCS predicted by the hard-ellipse model for (a) $v = 5$, $j = 6.5$ and $v = 0$, $j = 6.5$; (b) $v = 5$, $j = 16.5$ and $v = 0$, $j = 16.5$; and (c) $v = 5$, $j = 20.5$ and $v = 0$, $j = 20.5$

Conclusion

A crossed molecular beam ion-imaging apparatus was used to study the effect of initial vibrational excitation of NO on

rotational energy-transfer collisions with Ar. Only small shifts in rotational rainbow maxima to smaller angles were observed in the scattering of vibrationally excited NO from Ar compared to the scattering of NO in the ground vibrational state from Ar. A hard-ellipse potential model was used to interpret the shifts in terms of the angular anisotropy in the intermolecular potential. The experimental observations are consistent with a slight increase in angular anisotropy in the intermolecular potential arising from the initial vibrational excitation of $v = 5$ in NO.

Acknowledgment. This work was supported by the Department of Energy, Basic Energy Sciences, under Grant DE-FG02-88ER13934. We thank Dr. Michael Westley for helpful comments.

References and Notes

(1) Klar, H. *J. Phys. B* **1973**, *6*, 2139−2149.
(2) Green, S.; Zare, R. N. *Chem. Phys.* **1975**, *7*, 62−72.
(3) Alexander, M. H. *J. Chem. Phys.* **1982**, *76*, 5974−5988.
(4) Alexander, M. H. *Chem. Phys.* **1985**, *92*, 337−344.
(5) Thuis, H.; Stolte, S.; Reuss, J. *Chem. Phys.* **1979**, *43*, 351−364.
(6) Sudbo, A. S.; Loy, M. M. T. *Chem. Phys. Lett.* **1981**, *82*, 135−137.
(7) Sudbo, A. S.; Loy, M. M. T. *J. Chem. Phys.* **1982**, *76*, 3646−3654.
(8) Andresen, P.; Joswig, H.; Pauly, H.; Schinke, R. *J. Chem. Phys.* **1982**, *77*, 2204−2205.
(9) Joswig, H.; Andresen, P.; Schinke, R. *J. Chem. Phys.* **1986**, *85*, 1904−1914.
(10) Islam, M.; Smith, I. W. M.; Wiebrecht, J. W. *J. Phys. Chem.* **1994**, *98*, 9285−9290.
(11) Islam, M.; Smith, I. W. M.; Wiebrecht, J. W. *J. Chem. Phys.* **1995**, *103*, 9676−9691.
(12) James, P. L.; Sims, I. R.; Smith, I. W. M. *Chem. Phys. Lett.* **1997**, *272*, 412−418.
(13) James, P. L.; Sims, I. R.; Smith, I. W. M.; Alexander, M. H.; Yang, M. *J. Chem. Phys.* **1998**, *109*, 3882−3897.
(14) Islam, M.; Smith, I. W. M.; Alexander, M. H. *Chem. Phys. Lett.* **1999**, *305*, 311−318.
(15) Alexander, M. H. *J. Chem. Phys.* **1993**, *99*, 7725−7738.
(16) van Leuken, J. J.; Van Amerom, F. H. W.; Bulthuis, J.; Snijders, J. G.; Stolte, S. *J. Phys. Chem.* **1995**, *99*, 15573−15579.
(17) Lin, A.; Antonova, S.; Tsakotellis, A. P.; McBane, G. C. *J. Phys. Chem. A* **1999**, *103*, 1198−1205.
(18) van Leuken, J. J.; Bulthuis, J.; Stolte, S.; Snijders, J. G. *Chem. Phys. Lett.* **1996**, *260*, 595−603.
(19) de Lange, M. J. L.; Drabbels, M.; Griffiths, P. T.; Bulthuis, J.; Stolte, S.; Snijders, J. G. *Chem. Phys. Lett.* **1999**, *313*, 491−498.
(20) Drabbels, M.; Wodtke, A. M.; Yang, M.; Alexander, M. H. *J. Phys. Chem. A* **1997**, *101*, 6463−6474.
(21) Keil, M.; Slankas, J. T.; Kuppermann, A. *J. Chem. Phys.* **1979**, *70*, 541−551.
(22) Suits, A. G.; Bontuyan, L. S.; Houston, P. L.; Whitaker, B. J. *J. Chem. Phys.* **1992**, *96*, 8618−8620.
(23) Bontuyan, L. S.; Suits, A. G.; Houston, P. L.; Whitaker, B. J. *J. Phys. Chem.* **1993**, *97*, 6342−6350.
(24) Yonekura, N.; Gebauer, C.; Kohguchi, H.; Suzuki, T. *Rev. Sci. Instrum.* **1999**, *70*, 3265−3270.
(25) Westley, M. S.; Lorenz, K. T.; Chandler, D. W.; Houston, P. L. *J. Chem. Phys.* **2001**, *114*, 2669−2680.
(26) Jons, S. D.; Shirley, J. E.; Vonk, M. T.; Giese, C. F.; Gentry, W. R. *J. Chem. Phys.* **1992**, *97*, 7831−7834.
(27) Jons, S. D.; Shirley, J. E.; Vonk, M. T.; Giese, C. F.; Gentry, W. R. *J. Chem. Phys.* **1996**, *105*, 5397−5407.
(28) Yang, M.; Alexander, M. H. *J. Chem. Phys.* **1995**, *103*, 6973−6983.
(29) Alexander, M. H. *J. Chem. Phys.* **1999**, *111*, 7426−7434; Kohguchi, H.; Suzuki, T.; Alexander, M. H. *Science* **2001**, *294*, 832−834.
(30) Kim, Y.; Fleniken, J.; Meyer, H.; Alexander, M. H.; Dagdigian, P. J. *J. Chem. Phys.* **2000**, *113*, 73−85.
(31) Alexander, M. H.; Stolte, S. *J. Chem. Phys.* **2000**, *112*, 8017−8026.
(32) Ziegler, G.; Kumar, S. V. K.; Rubahn, H. G.; Kuhn, A.; Sun, B.; Bergmann, K. *J. Chem. Phys.* **1991**, *94*, 4252−4259.
(33) Eppink, A. T. J. B.; Parker, D. H. *Rev. Sci. Instrum.* **1997**, *68*, 3477−3484.
(34) Westley, M. S. Molecular Beam Studies of Inelastic and Reactive Scattering, Ph.D. Thesis, Cornell University, 2000.
(35) Pisano, P. J.; Westley, M. S.; Houston, P. L. *Chem. Phys. Lett.* **2000**, *318*, 385−392.
(36) Luque, L.; Crosley, D. R. Report MP 99-009; SRI International: Menlo Park, CA, 1999.
(37) Danielak, J.; Domin, U.; Kepa, R.; Rytel, M.; Zachwieja, M. *J. Mol. Spectrosc.* **1997**, *181*, 394−402.
(38) Bosanac, S. *Phys. Rev. A* **1980**, *22*, 2617−2622.
(39) Bosanac, S.; Buck, U. *Chem. Phys. Lett.* **1981**, *81*, 315−319.